Two-dimensional model for reactive-sorption columns of cylindrical geometry: Analytical solutions and moment analysis

Farman U Khan[a,c], Shamsul Qamar[a,b,*]

[a]Department of Mathematics, COMSATS Institute of Information Technology, Park Road, Chak Shahzad Islamabad, Pakistan

[b]Max Planck Institute for Dynamics of Complex Technical Systems, Sandtorstrasse 1, 39106 Magdeburg, Germany

[c]Department of Mathematics, Heavy Industry Taxila Education City (HITEC) Institute of Information Technology, Taxila, Pakistan

**Corresponding Author Email: shamsul.qamar@comsats.edu.pk*

Abstract

A set of analytical solutions are presented for a model describing the transport of a solute in a fixed-bed reactor of cylindrical geometry subjected to the first (Dirichlet) and third (Danckwerts) type inlet boundary conditions. Linear sorption kinetic process and first order decay are considered. Cylindrical geometry allows the use of large columns to investigate dispersion, adsorption/desorption and reaction kinetic mechanisms. The finite Hankel and Laplace transform techniques are adopted to solve the model equations. For further analysis, statistical temporal moments are derived from the Laplace transformed solutions. The developed analytical solutions are compared with the numerical solutions of high resolution finite volume scheme. Different case studies are presented and discussed for a series of numerical values corresponding to a wide range of mass-transfer and reaction kinetics. A good agreement was observed in the analytical and numerical concentration profiles and moments. The developed solutions are efficient tools for analyzing numerical algorithms, sensitivity analysis and simultaneous determination of the longitudinal and transverse dispersion coefficients from a laboratory-scale radial column experiment.

Key words: Two-dimensional model, equilibrium transport, reactive adsorption/desorption, first order decay, analytical solutions, moment analysis.

1. Introduction

Packed-bed reactors have wide range applications in gas, oil, and petrochemical industries, especially for solid-catalyzed heterogeneous reactions in which the packing serves as a catalyst. Fixed-bed absorbers/desorbers have high demand in various process industries, for example chromatography, where traditional separation operations like distillation, solvent extraction, crystallization and evaporation are not applicable due to physicochemical limitations.

Inside a chromatographic reactor the conversion of reactants and the separation of components take place simultaneously. The technique is useful to effectively reduce capital investment, energy and operating cost, equipment size, waste and pollution, as well as improves selectivity, purity, and productivity. This process has gained industrial popularity in the past few decades. For further details about the principles and applications of chromatographic reactors see [1–5]. The main motivation of this field of research is to provide profound insights into all aspects to scale up the process for industrial applications.

Mathematical modeling plays an important role in describing dynamical processes inside packed-bed reactors. It provides a procedure for predicting the dynamical behavior of solute in the reactor without extensive experiments. Because of different considerations of simplifications, several types of models have been developed and applied to illustrate the behavior of profiles inside the packed bed-reactors. Such models include the general rate model, the lumped kinetic model, the linear driving force model, the linear model, and the equilibrium dispersive model [6-8]. Each model has its own level of complexity to describe the process.

Analytical studies of the packed-bed reactor models are useful to understand the transport mechanism and to estimate chemical-physical parameters by the analysis of experimental data. Analytical solutions not only could shed some light on the physics of the problems, but also could be used for validation of numerical solutions for more elaborate and complex models, particularly in lack of experimental data.

A number of analytical solutions for one-, two- and three-dimensional advection-dispersion equations (ADEs) have been developed for predicting the transport of various contaminants in the subsurface. For example, several analytical solutions of the one-dimensional ADE were formulated in [9] subjected to various initial and boundary conditions. In [10–12] the authors have presented analytical solutions of the two-dimensional ADE with various source boundary conditions. The analytical solutions for three-dimensional ADE were derived in [13, 14]. However, these models were mostly limited to ADE in Cartesian coordinates with steady uniform flow [14]. Analytical solutions for two dimensional ADE in cylindrical coordinates are particularly useful for analyzing problems of the two-dimensional solute transport in a porous medium system with steady uniform flow [14–20].

The considered model could be efficiently applied when laboratory-scale experiment is performed in a cylindrical column. This is a practicable way of estimating transversal and longitudinal dispersion coefficients simultaneously.

Transverse dispersion coefficient is usually evaluated by interpreting steady-state transverse concentration profiles of conservative solutes in parallel flow [21, 22]. It has been inferred also from transient transport in column and parallel flow [23, 24]. In [23] the authors haves used the solution of the concentration profile computed on the column axe under the hypothesis that the edge of the column is so distant from its axes that it does not affect the profile.

It was concluded in [25] that kinematic waves can be partially characterized by mean and variance. This method, called moment analysis, has successfully quantified the physical properties of several products. It is an effective method for deducing important information about the retention equilibrium and mass transfer kinetics in a chromatographic column. Provided analytical solutions of the column mass balances are available, condensed information in the form of moments of the outlet profiles can be easily obtained. Moment analysis has been comprehensively discussed in the literature [26–39].

This manuscript presents a set of comprehensive analytical solutions for a two-dimensional model describing the transport of a single solute in a fixed-bed reactor. The current solutions extend our recent solutions of two-dimensional models for non-reactive flows inside fixed-bed columns [20, 40]. General solutions are derived for the solute concentration by applying finite Hankel transform together with Laplace transform [18, 19]. The finite Hankel transform technique is utilized to eliminate the radial coordinate, followed by the application of the Laplace transform to solve the resulting partial differential equation assuming both first (Dirichlet) and third-type (Danckwerts) inlet boundary conditions (BCs), linear sorption kinetic process, and first order decay or desorption-like reaction. Danckwerts BC is the more general BC and is important for large values of the axial dispersion coefficient, as it accounts for back mixing at the column inlet. On the other hand, Dirichlet BC is the simplest one and is useful when axial dispersion is small. The solutions of both BCs coincide for small axial dispersion (or large Peclet number). For further analysis, statistical temporal moments are derived from the Laplace transformed solutions. Typical examples of concentration profiles and moments resulting from different sets of inlet conditions are presented and briefly discussed. The analytical solutions are validated against the numerical solutions of high resolution finite volume scheme [41]. Good agreements in the results verify the correctness of analytical solutions and accuracy of the proposed numerical algorithm.

The complex interplay between thermodynamic and kinetic parameters renders the prediction of the reactor performance and the identification of suitable operating conditions is very difficult. The derived analytical solutions and moments could be very useful for further developments of fixed-bed reactors. In many situations sample sizes are small and diluted conditions hold. Therefore, linear assumptions are valid. Thus, our results can be used to study the effects of mass transfer and reaction kinetics on the elution profiles, for sensitivity analysis, for determining longitudinal and radial dispersion coefficients, and for determining reaction rate parameters from experimentally determined moments, among others. The studied 2D-model is more general and flexible compared to the classical 1D-models [39].

The current 2D model and solutions could be useful in various scenarios, for instance (a) the injection at the column inlet is not perfect (i.e. a radial profile is introduced at the column inlet), (b) the column is not homogeneously packed (which is more probable in the case of larger columns), (c) radial temperature gradients exist, also related to radial concentration gradients. All such situations can happen in reality. Often they might be minor and even negligible, then, 1D are justified. However, for their relevance and effects 2D models are required. With current isothermal model we could just study case (a) by assuming injections in inner cylinders or outer annuli. Cases (b) and (c) are more complicated and require further model extensions (considering non-constant column porosities and an energy balance).

The structure of the article is as follows: The two-dimensional mathematical model for reactive-sorption columns of cylindrical geometry is described in Section 2. Section 3 presents the derivation of analytical solutions. Section 4 presents the temporal moments. Numerical test problems are presented in Section 5. Concluding remarks are given in Section 6.

2. Mathematical Model

This study considers the transport of a solute in a two-dimensional chromatographic reactor of radial geometry as illustrated schematically in Figure 1.

The injected solute migrates in the *z*-direction by advection and axial dispersion, spreads in the *r*-direction by radial dispersion, and decays due to first order chemical reaction. We neglect in this study flow rate variations and keep the interstitial velocity u as constant. It is further assumed that solute undergoes linear adsorption and chemical reaction is represented by first order kinetics. To trigger and amplify the effect of possible rate limitations of the mass transfer in the radial direction, the following specific injection conditions are assumed. By introducing a parameter $\widetilde{r}$ the inlet cross section of the column is divided into an inner cylindrical core and an outer annular ring (see Figure 1). The injection profile is formulated in a general way allowing for injection either through an inner core, an outer ring or through the whole cross section. The latter case results if $\widetilde{r}$ is set equal to the radius of the column denoted by R. Since in the latter case no initial radial gradients are provided, the solutions should converge into the solution of the simpler one-dimensional model [39].

Based on the above setup, the governing equation of a single-solute two-dimensional linear reactive equilibrium

dispersive model (EDM) for a fixed bed chromatographic column can be expressed as

$$(1+aF)\frac{\partial c}{\partial t}+u\frac{\partial c}{\partial z}=D_z\frac{\partial^2 c}{\partial z^2}+D_r\left(\frac{\partial^2 c}{\partial r^2}+\frac{1}{r}\frac{\partial c}{\partial r}\right)-\mu c. \quad (1)$$

Here, $F=(1-\varepsilon)/\varepsilon$ is phase ratio based on the porosity $\varepsilon\in(0,1)$, μ is the first order decay constant, $c(r,z,t)$ denotes concentration of the solute, t is time, and D_z and D_r represent the longitudinal and radial dispersion coefficients, respectively.

To simplify the analysis, let us define some dimensionless variables

$$x=\frac{z}{L},\ \tau=\frac{tu}{L(1+aF)},\ \rho=\frac{r}{R},\ Pe_z=\frac{Lu}{D_z},\ Pe_r=\frac{R^2u}{D_rL},\ \kappa=\frac{\mu L}{u}. \quad (2)$$

Here L is the length of the column. Using these variables in Eq. (1), we have

$$\frac{\partial c}{\partial \tau}=\frac{1}{Pe_z}\frac{\partial^2 c}{\partial x^2}-\frac{\partial c}{\partial x}+\frac{1}{Pe_r}\left(\frac{\partial^2 c}{\partial \rho^2}+\frac{1}{\rho}\frac{\partial c}{\partial \rho}\right)-\kappa c. \quad (3)$$

The corresponding initial condition is given by

$$c(\rho,x,\tau=0)=c_{init},\quad 0\le x\le 1,\ \ 0\le\rho\le 1, \quad (4)$$

where c_{init} is the initial concentration of the solute in the column. The boundary conditions subjected to the above equation at $\rho=0$ and $\rho=1$ are given as

$$\frac{\partial c(\rho=1,x,\tau)}{\partial\rho}=0,\qquad \frac{\partial c(\rho=0,x,\tau)}{\partial\rho}=0. \quad (5)$$

Moreover, the two sets of boundary condition at the column inlet and outlet are summarized below.

Case 1: Concentration pulse of finite width injected as Dirichlet inlet BCs:

For injection in the inner circular region, it is expressed as

$$c(\rho,x=0,\tau)=\begin{cases}c_{i,inj}, & \text{if } 0\le\rho\le\tilde{\rho} \text{ and } 0\le\tau\le\tau_{inj}\\ 0 & \tilde{\rho}<\rho<1 \text{ or } \tau>\tau_{inj}\end{cases} \quad (6)$$

while, for injection in the outer annular zone, we have

$$c(\rho,x=0,\tau)=\begin{cases}c_{i,inj}, & \text{if } \rho\le\tilde{\rho}\le 1 \text{ and } 0\le\tau\le\tau_{inj}\\ 0, & 0\le\rho\le\tilde{\rho} \text{ or } \tau>\tau_{inj}.\end{cases} \quad (7)$$

Here, c_{inj} is the concentration of injected solute solution, τ_{inj} is the time of injection and

$$\tilde{\rho}=\frac{\tilde{r}}{R}, \quad (8)$$

where $\tilde{r}$ represents the radius of inner spherical core as shown in Figure 1.For injection over the whole inlet cross section of the column, either $\tilde{\rho}=1$ in Eq. (6) or $\tilde{\rho}=0$ in Eq. (7).

At the column outlet, the useful and realistic Neumann BCs for hypothetically infinite column length (Neumann at infinity) is given as

$$\left.\frac{\partial c}{\partial x}\right|_{x=\infty}=0. \quad (9)$$

Case 2: Concentration pulse of finite width injected as Danckwerts inlet BCs:

For the inner zone injection, this boundary condition is expressed as

$$c(\rho,x=0,\tau)-\frac{1}{Pe_z}\frac{\partial c(\rho,0,\tau)}{\partial x}=\begin{cases}c_{iinj}, & \text{if } 0\le\rho\le\tilde{\rho} \text{ and } 0\le\tau\le\tau_{inj},\\ 0, & \tilde{\rho}<\rho<1 \text{ or } \tau>\tau_{inj},\end{cases} \quad (10)$$

while, for injection in the outer annular zone, we have

$$c(\rho,0,\tau)-\frac{1}{Pe_z}\frac{\partial c(\rho,x=0,\tau)}{\partial x}=\begin{cases}c_{iinj}, & \text{if } \rho\le\tilde{\rho}\le 1 \text{ and } 0\le\tau\le\tau_{inj}\\ 0, & 0\le\rho\le\tilde{\rho} \text{ or } \tau>\tau_{inj},\end{cases} \quad (11)$$

together with Neumann condition at the outlet of the column

$$\left.\frac{\partial c}{\partial x}\right|_{x=1}=0. \quad (12)$$

3. Derivation of analytical solution

The chromatographic model in Eq. (3) and its associated initial and boundary conditions are analytically solved by successive implementation of the finite Hankel transform and the Laplace transform, see [18, 19]. The Hankel transformation of Eq. (3) with respect to ρ gives

$$\frac{\partial c_H}{\partial \tau}=\frac{1}{Pe_z}\frac{\partial^2 c_H}{\partial x^2}-\frac{\partial c_H}{\partial x}-\left(\frac{\lambda_n^2}{Pe_r}+\kappa\right)c_H, \quad (13)$$

where λ_n is the finite Hankel transform parameter as determined by the transcendental equation $\frac{dJ_0(\lambda_n)}{d\rho}=-J_1(\lambda_n)=0$. Here $j_0(.)$ and $j_1(.)$ are the zeroth and first order Bessel functions of the first kind and $c_H(\lambda_n,x,\tau)$ is the finite Hankel transform for $c(\rho,x,\tau)$ as defined by the following conjugate equation

$$c_H(\lambda_n,x,\tau)=H[c(\rho,x,\tau)]=\int_0^1\rho c(\rho,x,\tau)J_0(\lambda_n\rho)d\rho, \quad (14)$$

$$c(\rho,x,\tau)=2c_H(\lambda_n=0,x,\tau)+2\sum_{n=1}^{\infty}c_H(\lambda_n,x,\tau)\frac{J_0(\lambda_n\rho)}{\left|J_0(\lambda_n)\right|^2}. \quad (15)$$

Accordingly, the initial condition in Eq. (4) after the finite Hankel transform becomes

$$c_H(\lambda_n,x,\tau=0)=c_{init}F(\lambda_n). \quad (16)$$

For injection at the inner cylindrical core, we have

$$F(\lambda_n) = \begin{cases} \frac{\tilde{\rho}^2}{2}, & \text{if} \quad \lambda_n = 0, \\ \frac{\tilde{\rho}}{\lambda_n} J_1(\lambda_n \tilde{\rho}), & \text{if} \quad \lambda_n \neq 0. \end{cases} \tag{17}$$

While, for injection at the outer annular ring, it becomes

$$F(\lambda_n) = \begin{cases} \left(\frac{1}{2} - \frac{\tilde{\rho}^2}{2}\right), & \text{if} \quad \lambda_n = 0, \\ -\frac{\tilde{\rho}}{\lambda_n} J_1(\lambda_n \tilde{\rho}), & \text{if} \quad \lambda_n \neq 0. \end{cases} \tag{18}$$

The value of $\tilde{\rho}$ is given by Eq. (8). By applying Laplace transformation on Eq. (13) with respect to t, we have

$$\frac{\partial^2 \bar{c}_H}{\partial x^2} - Pe_z \frac{\partial \bar{c}_H}{\partial x} - Pe_z\left(\frac{\lambda_n^2}{Pe_r} + \kappa + s\right)\bar{c}_H = -c_{init} F(\lambda_n) Pe_z \tag{19}$$

The general solution of this equation comes out to be

$$\bar{c}_H = A_0 e^{m_1 x} + B_0 e^{m_2 x} + \frac{c_{init} F(\lambda_n)}{\left(\frac{\lambda_n^2}{Pe_r} + \kappa + s\right)}, \tag{20}$$

$$m_{1,2} = \frac{Pe_z}{2} \pm \sqrt{\left(\frac{Pe_z}{2}\right)^2 + Pe_z\left(\frac{\lambda_n^2}{Pe_r} + \kappa + s\right)}. \tag{21}$$

The constants A_0 and B_0 are to be determined from the boundary conditions.

Case 1: Concentration pulse of finite width injected as Dirichlet inlet BCs:

The Hankel transformations of Eq. (6)(or Eq. (7)) and Eq. (9) are given as

$$c_H(\lambda_n, x=0, \tau) = \begin{cases} c_{inj} F(\lambda_n), & \text{if } 0 \le \tau \le \tau_{inj}, \\ 0, & \tau > \tau_{inj} \end{cases} \tag{22}$$

$$\left.\frac{\partial c_H(\lambda_n, x, \tau)}{\partial x}\right|_{x=\infty} = 0. \tag{23}$$

where $F(\lambda_n)$, for inner and outer annular injections, are given by Eqs. (17) and (18). After applying Laplace transformation on the boundary conditions in Eqs. (22) and (23), we obtain

$$\bar{c}_H(\lambda_n, x=0, s) = \frac{c_{inj} F(\lambda_n)}{s}\left(1 - e^{-s\tau_{inj}}\right), \left.\frac{\partial \bar{c}_H}{\partial x}\right|_{x=\infty} = 0 \tag{24}$$

Using Eq. (24) in Eq. (20), we obtain

$$A_0 = 0, B_0 = \frac{c_{inj} F(\lambda_n)}{s}\left(1 - e^{-s\tau_{inj}}\right) - \frac{c_{init} F(\lambda_n)}{\left(\frac{\lambda_n^2}{Pe_r} + \kappa + s\right)}. \tag{25}$$

After using the values of A_0 and B_0, the solution of Eq. (20) becomes

$$\bar{c}_H(\lambda_n, x, s) = \left(\frac{c_{inj}(1 - e^{-s\tau_{inj}})}{s} - \frac{c_{init}}{\frac{\lambda_n^2}{Pe_r} + \kappa + s}\right) F(\lambda_n) e^{m_2 x} + \frac{c_{init} F(\lambda_n)}{\frac{\lambda_n^2}{Pe_r} + \kappa + s}, \tag{26}$$

where the value of m_2 is given in Eq. (21). Using the inverse Laplace transformation on Eq. (26), the solution in actual time domain is given as

$$c_H(\lambda_n, x, \tau) = \begin{cases} A(\lambda_n, x, \tau), & 0 \le \tau \le \tau_{inj}, \\ A(\lambda_n, x, \tau) - A(\lambda_n, x, \tau - \tau_{inj}), & \tau \ge \tau_{inj}, \end{cases} \tag{27}$$

where, for $v = \sqrt{Pe_z^2 + 4Pe_z\left(\frac{\lambda_n^2}{Pe_r} + \kappa\right)}$,

$$A(\lambda_n, x, \tau) = \frac{c_{inj} F(\lambda_n)}{2} e^{\frac{(Pe_z - v)x}{2}} \operatorname{erfc}\left(\frac{Pe_z x - v\tau}{2\sqrt{Pe_z \tau}}\right) + \frac{c_{inj} F(\lambda_n)}{2} e^{\frac{(Pe_z + v)x}{2}} \operatorname{erfc}\left(\frac{Pe_z x + v\tau}{2\sqrt{Pe_z \tau}}\right) - \frac{c_{init} F(\lambda_n) e^{-\left(\frac{\lambda_n^2}{Pe_r} + \kappa\right)\tau}}{2}\left[\operatorname{erfc}\left(\frac{x - \tau}{2\sqrt{\frac{\tau}{Pe_z}}}\right) + e^{Pe_z x} \operatorname{erfc}\left(\frac{x + \tau}{2\sqrt{\frac{\tau}{Pe_z}}}\right) - 2\right]. \tag{28}$$

Case 2: Concentration pulse of finite width injected as Danckwerts inlet BCs:

The Hankel transformations of Eq. (10) (or Eq. (11)) and Eq. (12) are given as

$$c_H(\lambda_n, x=0, \tau) = \frac{1}{Pe_z}\frac{\partial c_H(\lambda_n, x=0, \tau)}{\partial x} + \begin{cases} c_{inj} F(\lambda_n), & 0 \le \tau \le \tau_{inj}, \\ 0, & \tau \ge \tau_{inj}, \end{cases} \tag{29}$$

together with the Neumann condition at the outlet of the column

$$\left.\frac{\partial c_H(\lambda_n, x, \tau)}{\partial x}\right|_{x=1} = 0. \tag{30}$$

Once again $F(\lambda_n)$, for inner and outer annular injections, are given by Eq. (17) and Eq. (18).

After applying the Laplace transformation on these boundary conditions, we get

$$\bar{c}_H(\lambda_n, x=0, s) = \frac{1}{Pe_z}\frac{\partial \bar{c}_H(\lambda_n, x=0, s)}{\partial x} + \frac{c_{inj} F(\lambda_n)}{s}\left(1 - e^{-s\tau_{inj}}\right), \tag{31}$$

and

$$\left.\frac{\partial \bar{c}_H}{\partial x}\right|_{x=1} = 0. \tag{32}$$

Now using Eqs. (31) and (32) in Eq.(20), we obtain

$$A_0 = \frac{m_2 e^{m_2}\left(\dfrac{c_{inj}F(\lambda_n)}{s}\left(1-e^{-s\tau_{inj}}\right)-\dfrac{c_{init}F(\lambda_n)}{\dfrac{\lambda_n^2}{Pe_r}+\kappa+s}\right)}{m_2 e^{m_2}\left(1-\frac{m_1}{Pe_z}\right)-m_1 e^{m_1}\left(1-\frac{m_2}{Pe_z}\right)}, \quad (33)$$

$$B_0 = \frac{m_1 e^{m_1}\left(\dfrac{c_{inj}F(\lambda_n)}{s}\left(1-e^{-s\tau_{inj}}\right)-\dfrac{c_{init}F(\lambda_n)}{\dfrac{\lambda_n^2}{Pe_r}+\kappa+s}\right)}{m_1 e^{m1}\left(1-\frac{m2}{Pe_z}\right)-m_2 e^{m2}\left(1-\frac{m_1}{Pe_z}\right)}. \quad (34)$$

Thus the solution in Eq. (20) takes the form

$$\bar{c}_H(\lambda_n,x,s)=\frac{F(\lambda_n)\left(m_2 e^{m_2+m_1 x}-m_1 e^{m_1+m_2 x}\right)\left(\dfrac{c_{inj}}{s}\left(1-e^{-s\tau_{inj}}\right)-\dfrac{c_{init}}{\dfrac{\lambda_n^2}{Pe_r}+\kappa+s}\right)}{m_2 e^{m_2}\left(1-\frac{m_1}{Pe_z}\right)-m_1 e^{m_1}\left(1-\frac{m_2}{Pe_z}\right)} + \frac{c_{init}F(\lambda_n)}{\frac{\lambda_n^2}{Pe_r}+\kappa+s}. \quad (35)$$

No analytical inverse Laplace transformation is possible to bring back the solution in the actual time domain $c(\rho, x, \tau)$. For that reason numerical Laplace inversion will be used to get the solution in actual time domain, see [42]. In this method the integral of inverse Laplace transform is replaced by Fourier series.

4. Moment Analysis

Moment analysis is known to be an effective method for deducing important information about the retention equilibrium and mass transfer kinetics in a chromatographic column. It can be applied in various ways, namely (a) to describe in a simpler manner essential features of the chromatograms, (b) to estimate efficiently free model parameters by matching measured and predicted moments, (c) to efficiently predict performance parameters of the separations and, thus, (d) to optimize more easily the process. In this study, we addressed essentially just the aspect (a). The zeroth moment describes the peak area (mass), the first moment corresponds to the retention time, the second central moment or variance provides significant information related to mass transfer processes in the column, while the third central moment analyzes the fronts asymmetries (skewness). The experimental values measured for these moments can be compared with their theoretical expressions to estimate dispersion and other mass transfer coefficients. Normalized averaged *i*-th moments of the band profile at any position in the column can be obtained through the following expression

$$\mu_{i,av} = \frac{\int_0^\infty c_{av}(x,\tau)\,\tau^i d\tau}{\mu_{0,av}}, \quad i = 1,2,3,\cdots, \quad (36)$$

where

$$c_{av}(x,\tau) = 2\int_0^1 c(\rho,x,\tau)\,\rho\, d\rho, \quad (37)$$

and for the zeroth moment (mass balance) holds

$$\mu_{0,av} = \int_0^\infty c_{av}(x,\tau)\,d\tau. \quad (38)$$

Due to mass balance consideration for this zeroth moment holds

$$\mu_{0,av} = c_{inj,av}\tau_{inj}, \quad (39)$$

where $c_{inj,av} = c_{inj}\tilde{\rho}^2$ for the inner circular zone injection and $c_{inj,av} = c_{inj}\left(1-\tilde{\rho}^2\right)$ for the outer annular zone injection. Moreover, according to Eq. (2), $\tau_{inj} = \frac{ut_{inj}}{L(1+aF)}$.

When mass transfer in the radial direction is assumed hypothetically to be infinitely fast, $c_{av}(x,\tau) = c(\rho,x,\tau)$, that corresponds to the 1D case presented in [39]. Due to its moment generating properties the Laplace transformation can be used as a basic tool to derive analytical expressions for the moments. In this study, analytical temporal moments are derived as functions of radial coordinate ρ at the outlet of the column $(x=1)$ considering $c_{init}=0$. Afterwards, these moments are used to obtain the aforementioned averaged moments by integrating over ρ. The following property of the Laplace transform was used to determine the analytical moments from the Laplace and Hankel transformed concentration $\bar{c}_H$ in Eq. (26) or Eq. (35):

$$\mu_{i,H} = (-1)^i \lim_{s\to 0}\frac{d^i(\bar{c}_H(\lambda_n,x,s))}{ds^i}, \quad i = 0,1,2,\cdots. \quad (40)$$

The actual moments $\mu_i(\rho)$ are generated from Eq. (15) by taking moments of the concentrations on both sides of that relation. On multiplying both sides of Eq. (15) with τ^i and integrating over τ from 0 to ∞, we obtain

$$\mu_i(\rho) = 2\mu_{i,H}(\lambda_n=0) + 2\sum_{n=1}^{\infty}\mu_{i,H}(\lambda_n)\frac{J_0(\lambda_n\rho)}{|J_0(\lambda_n)|^2}. \quad (41)$$

From the above moments, the averaged non-normalized temporal moments $M_{i,av}$ can be calculated as

$$M_{i,av} = 2\int_0^1 \mu_i(\rho)\,\rho\, d\rho, \quad i = 0,1,2,\cdots. \quad (42)$$

Finally, the normalized averaged temporal moments (c.f. Eq. (36)) which are widely used in chemical engineering are available as [39]

$$\mu_{i,av} = \frac{M_{i,av}}{\mu_{0,av}}, \quad \mu_{0,av} = M_{0,av}, \quad i = 1,2,3,\cdots. \quad (43)$$

For evaluation of the solute transport behaviour, the above averaged temporal moments $\mu_{i,av}$ up to the fourth order are derived. These moments can be used to get finally also the first three averaged central moments defined below (see [39]):

$$\mu'_{2,av} = \mu_{2,av} - \mu^2_{1,av}.$$
$$\mu'_{3,av} = \mu_{3,av} - 3\mu_{1,av}\mu_{2,av} + 2\mu^3_{1,av}. \quad (44)$$
$$\mu'_{4,av} = \mu_{4,av} - 4\mu_{1,av}\mu_{3,av} + 6\mu^2_{1,av}\mu_{2,av} - 3\mu^4_{1,av}.$$

The corresponding *i*-th central moments of the band profile at the outlet of a column of length $x = 1$ are numerically obtained using the expression

$$\mu'_{i,av} = \frac{\int_0^\infty c_{av}(x=1,\tau)(\tau-\mu_1)^i d\tau}{\mu_{0,av}}, \quad i = 2,3,4,\cdots, \quad (45)$$

where, $\mu_{0.av}$ for $x = 1$ is given by Eq. (38). The trapezoidal rule is applied to numerically approximate the integrals in Eqs. (36)-(38) and (45). The central moments are well known in chemical engineering due to their physical meanings [39]. Hereby the zeroth moment corresponds to mass balance (peak areas), the first to mean retention times, the second to variance around the mean resentence time, the third to peak asymmetry (skewness) and the forth to kurtosis. The values of these moments should be in agreement with those provided in[39] based on an analysis of the 1D case, in which D_z has an effect on their values.

Case 1: Dirichlet inlet BC (Eq. (6) or (7) and (9))

The moments of $\bar{c}_H$ in Eq. (26) are given below.

The zeroth moment: According to Eq. (26) and Eq. (40) for $i = 0$, the zeroth moment is given as

$$\mu_{0,H} = \tau_{inj} c_{inj} F(\lambda_n) \exp\left(\frac{Pe_z - v}{2}\right),$$
$$\text{where } v = \sqrt{Pe_z^2 + 4Pe_z\left(\frac{\lambda_n^2}{Pe_r} + \kappa\right)}. \quad (46)$$

Here, $F(\lambda_n)$ is given by Eq. (17) for inner zone injection and by Eq. (18) for outer annular zone injection.

First moment: The first moment is calculated from Eq. (26) and Eq. (40) for $i = 1$ and is expressed as

$$\mu_{1,H} = \left[\frac{\tau_{inj}}{2} + \frac{Pe_z}{v}\right]\mu_{0,H}. \quad (47)$$

Second moment: The second moment is given as

$$\mu_{2,H} = \left[\frac{\tau_{inj}^2}{3} + \frac{\tau_{inj}}{v}Pe_z + \frac{Pe_z^2(2+v)}{v^3}\right]\mu_{0,H}. \quad (48)$$

Third moment: The third moment of Eqs. (26) is given as

$$\mu_{3,H} = \frac{\tau_{inj}^3}{4} + \tau_{inj}^2\frac{Pe_z}{v} + \frac{3\tau_{inj}}{2}Pe_z^2\left(\frac{2+v}{v^3}\right) + Pe_z^3\frac{(v^2+6v+12)}{v^5}. \quad (49)$$

Fourth moment: Similarly the fourth moment comes out to be

$$\mu_{4,H} = \frac{Pe_z^4}{v^7}(v^3+12v^2+60v+120) + \frac{2\tau_{inj}Pe_z^3}{v^5}(v^2+6v+12) + \frac{2\tau_{inj}^2Pe_z^2}{v^3}(2+v) + \frac{\tau_{inj}^3Pe_z}{v} + \frac{\tau_{inj}^4}{5} \quad (50)$$

Case 2: Dankwerts inlet BC (Eqs. (10) or (11) and (12))

The temporal moments of concentration profile given by Eq. (35) are calculated using Eq. (40).

The zeroth moment: It is given as

$$\mu_{0,H} = \frac{c_{inj}F(\lambda_n)\tau_{inj}ve^{Pe_z}}{\left((\alpha+\beta)e^{\lambda_1} - (\alpha-\beta)e^{\lambda_2}\right)}, \quad \beta = \frac{1}{2}v, \quad (51)$$

and v is given by Eq. (46). Moreover,

$$\alpha = \frac{Pe_z}{2} + \frac{\lambda_n^2}{Pe_r} + \kappa, \quad \lambda_{1,2} = \frac{Pe_z \pm v}{2}. \quad (52)$$

First moment:

$$\mu_{1,H} = \frac{[Pe_z(\alpha_3-\alpha_2)-\alpha_1]e^{\lambda_2} - [Pe_z(\alpha_3+\alpha_2)+\alpha_1]e^{\lambda_1}}{2\alpha_4\left((\alpha-\beta)e^{\lambda_2} - (\alpha+\beta)e^{\lambda_1}\right)}\mu_{0,H} \quad (53)$$

where

$$\alpha_1 = \frac{Pe_r^2(1+\tau_{inj})}{8}\left(Pe_z^2 + 4Pe_z\left(\frac{\lambda_n^2}{Pe_r} + \kappa\right)\right)^{\frac{3}{2}},$$
$$\alpha_2 = \frac{Pe_zPe_r^2}{8}\sqrt{Pe_z^2 + 4Pe_z\left(\frac{\lambda_n^2}{Pe_r} + \kappa\right)},$$
$$\alpha_3 = \frac{Pe_r^2}{8}\left[(\tau_{inj}+2)Pe_z^2 + (6\tau_{inj}+8)\kappa Pe_z + \kappa^2\tau_{inj} + \kappa\right] + \frac{\lambda_n^2Pe_r}{4}\left((4+3\tau_{inj})Pe_z + 8\kappa\tau_{inj} + 4\right) + \lambda_n^4\tau_{inj},$$
$$\alpha_4 = \left(\left(\frac{Pe_z}{4} + \kappa\right)Pe_z + \frac{\lambda_n^2}{Pe_r}\right).$$

Similarly the second moment comes out to be

Second moment:

$$\mu_{2,H} = \left[\frac{\left[12\tau_{inj}^2\left((\alpha_6-\alpha_5)e^{\lambda_3} - (\alpha_6+\alpha_5)e^{\lambda_4} - \alpha_7\right) + 9\tau_{inj}\left((\alpha_9-\alpha_8)e^{\lambda_3} - (\alpha_9+\alpha_8)e^{\lambda_4} - \alpha_{10}\right)\right]}{4\beta_1Pe_r^2\left((\alpha-\beta)e^{\lambda_2} - (\alpha+\beta)e^{\lambda_1}\right)^2} + \frac{3Pe_r\left((\alpha_{11}-\alpha_{12})e^{\lambda_4}\right) + \left((\alpha_{11}+\alpha_{12})e^{\lambda_3}\right) + 2\alpha_{13}}{2\beta_1Pe_r^2\left((\alpha-\beta)e^{\lambda_2} - (\alpha+\beta)e^{\lambda_1}\right)^2}\right]\mu_{0,H},$$
$$\beta_1 = \left(\left(\frac{Pe_z}{4} + \kappa\right)Pe_r + \lambda_n^2\right)^2\sqrt{Pe_z + 4\left(\kappa + \frac{\lambda_n^2}{Pe_r}\right)},$$
$$\lambda_{3,4} = Pe_z \pm v,$$

$$\alpha_5 = \frac{-1}{4}\left(\left(\frac{Pe_z}{4}+\kappa\right)Pe_r+\lambda_n^2\right)^2\left(\begin{array}{l}\left(\frac{Pe_z^2}{4}+\kappa^2+2Pe_z\kappa\right)Pe_r^2\\+2\lambda_n^2(Pe_z+\kappa)Pe_r+\lambda_n^4\end{array}\right)$$

$$\times\sqrt{Pe_z+4\left(\kappa+\frac{\lambda_n^2}{Pe_r}\right)},$$

$$\alpha_6 = \frac{\sqrt{Pe_z}Pe_r}{128}\Bigg(160\,(\kappa Pe_r+\lambda_n^2)^3\,Pe_z+72\,Pe_r(\kappa Pe_r$$

$$+\lambda_n^2)^2\,Pe_z^2+14\,Pe_r^2(\kappa Pe_r+\lambda_n^2)Pe_z^3+Pe_r^3Pe_z^4+$$

$$Pe_r^3\left(\kappa+\frac{\lambda_n^2}{Pe_r}\right)\Bigg),$$

$$\alpha_7 = \frac{1}{2}\left(\left(\frac{Pe_z}{4}+\kappa\right)Pe_r+\lambda_n^2\right)^2\sqrt{Pe_z+4\left(\kappa+\frac{\lambda_n^2}{Pe_r}\right)}$$

$$+Pe_r^2\left(\kappa+\frac{\lambda_n^2}{Pe_r}\right)e^{Pe_z},$$

$$\alpha_8 = -Pe_r\left(\frac{Pe_zPe_r}{4}+\kappa Pe_r+\lambda_n^2\right)\left[\begin{array}{l}\left(\kappa Pe_z+\frac{\kappa}{2}+\frac{Pe_z^2}{4}\right)Pe_r\\+Pe_z\lambda_n^2+\frac{\lambda_n^2}{2}\end{array}\right]$$

$$\left(\frac{Pe_rPe_z}{2}+\kappa Pe_r+\lambda_n^2\right)\sqrt{Pe_z+4\left(\kappa+\frac{\lambda_n^2}{Pe_r}\right)},$$

$$\alpha_9 = \frac{5\,Pe_r\,Pe_z^{\frac{3}{2}}}{2}\left(\kappa Pe_r+\lambda_n^2\right)^2\left(\kappa Pe_r+\frac{p_r}{5}+\lambda_n^2\right)$$

$$+\frac{25\,Pe_r^2\,Pe_z^{\frac{5}{2}}}{16}\left(\kappa Pe_r+\lambda_n^2\right)\left(KPe_r+\frac{Pe_r}{25}+\lambda_n^2\right)$$

$$+\frac{3\,Pe_r^3\,Pe_z^{\frac{7}{2}}}{8}\left(\kappa Pe_r+\lambda_n^2\right)+\frac{Pe_r^4\,Pe_z^{\frac{9}{2}}}{32}$$

$$+\sqrt{Pe_z}\left(\kappa Pe_r+\lambda_n^2\right)^3\left(\kappa Pe_r+Pe_r+\lambda_n^2\right),$$

$$\alpha_{10} = Pe_re^{Pe_z}\left(\kappa Pe_r+\lambda_n^2\right)\left(\frac{Pe_rPe_z}{4}+\kappa Pe_r+\lambda_n^2\right)$$

$$\left(\frac{Pe_rPe_z}{2}+\kappa Pe_r+\lambda_n^2\right)\sqrt{Pe_z+4\left(\kappa+\frac{\lambda_n^2}{Pe_r}\right)},$$

$$\alpha_{11} = Pe_r^3\left[\begin{array}{l}\frac{Pe_z\kappa^3}{6}+\left(\frac{2Pe_z}{3}+\frac{1}{2}+\frac{3Pe_z^2}{8}\right)\kappa^2+\frac{\kappa Pe_z^2}{6}(2+Pe_z)\\+\frac{Pe_z^2}{48}\left(Pe_z^2-2+2Pe_z\right)\end{array}\right]$$

$$+\frac{\lambda_n^2Pe_r^2}{2}\left(\kappa^2Pe_z+\kappa\left(2+\frac{3Pe_z^2}{2}+\frac{8Pe_z}{3}\right)+\frac{Pe_z^2}{3}(2+Pe_z)\right)$$

$$+\frac{1}{2}\left(\frac{3Pe_z^2}{4}+\frac{4Pe_z}{3}+\kappa Pe_z+1\right)\lambda_n^4Pe_r+\frac{Pe_z\lambda_n^6}{6}\Bigg)\sqrt{Pe_z+4\left(\kappa+\frac{\lambda_n^2}{Pe_r}\right)},$$

$$\alpha_{12} = \frac{2}{3}\left(\kappa Pe_r+\lambda_n^2\right)\left(\begin{array}{l}\left(15\kappa+8\kappa^2-1\right)\frac{Pe_r^2}{8}\\+\left(16\kappa+15\right)\frac{\lambda_n^2Pe_r}{8}+\lambda_n^4\end{array}\right)Pe_z^{\frac{3}{2}}+$$

$$\frac{2Pe_r}{3}\left(\left(10\kappa+16\kappa^2-1\right)\frac{Pe_r^2}{16}+\left(16\kappa+5\right)\frac{\lambda_n^2Pe_r}{8}+\lambda_n^4\right)Pe_z^{\frac{5}{2}}$$

$$+\frac{5Pe_r^2}{24}\left(\left(\kappa+\frac{1}{5}\right)Pe_r+\lambda_n^2\right)Pe_z^{\frac{7}{2}}+\frac{Pe_r^3Pe_z^{\frac{9}{2}}}{48}+$$

$$\left(\kappa Pe_r+\lambda_n^2\right)^2\sqrt{Pe_z}\left(\left(\kappa+\frac{1}{3}\right)Pe_r+\lambda_n^2\right),$$

$$\alpha_{13} = \left[\begin{array}{l}Pe_r^3\left(Pe_z\kappa^3+\left(\frac{Pe_z^2}{4}-2Pe_z-1\right)\kappa^2-\frac{\kappa Pe_z^2}{2}+\frac{Pe_z^2}{12}\right)\\+3\left(Pe_z\kappa^2+\left(\frac{Pe_z^2}{6}-\frac{4Pe_z}{3}-\frac{2}{3}\right)\kappa-\frac{Pe_z^2}{6}\right)\lambda_n^2Pe_r^2\\+3\left(\kappa Pe_z-\frac{1}{3}-\frac{2Pe_z}{3}+\frac{Pe_z^2}{12}\right)\lambda_n^4Pe_r+Pe_z\lambda_n^6\end{array}\right]$$

$$\times e^{Pe_z}\sqrt{Pe_z+4\left(\kappa+\frac{\lambda_n^2}{Pe_r}\right)}.$$

The expressions of $\mu_{3,H}$ and $\mu_{4,H}$ were very lengthy. Therefore, only plots of these moments will be presented in the considered test problems.

5. Numerical Test Problems

In this section, several case studies are carried out to validate the derived analytical solutions. For comparison, a second-order accurate finite volume scheme (FVS) is applied to numerically approximate the model equations (3)-(12) [41]. All parameters used in the test problems are given in Table 1, except the last problem in which experimental and analytical results are compared. It is import to mention that this study deals with dimensionless quantities in the model equations. Therefore, the general trends identified and discussed below also hold for larger column dimensions and additional calculations for a large scale would not bring new insight.

Rectangular concentration profiles

This series of calculations analyzes the influences of boundary conditions, types of injections, dispersion coefficients, and first order decay on the concentration profiles. The sample is either injected through the inner cylindrical core or the outer annular ring. In the calculations described here, the radius of inner cylindrical core $\tilde{r}$ is chosen in such a manner that the inner and outer annular zones have the same areas. Thus, for a column of radius $R=0.2$ the inner zone radius comes out to be $\tilde{r}=0.1414$ (or $\tilde{\rho}=0.707$). For validation, analytical solutions are compared with the numerical solutions of finite volume scheme [41].

A comparison of analytical and numerical solutions for different values of dimensionless reaction rate constant κ

and Pe_z is given in Figure 2 at $x=1$ for the case that the sample is injected at $x=0$ through the inner cylindrical core. In Figure 2 (top: left), Danckwerts BCs are considered with $Pe_z=20$ and $Pe_r=0.5$ are kept fixed. The local elution profiles in the centre $(\rho=0)$ are plotted for different values of reaction rate constants. Comparison of these results indicates that the presence of reaction in the mobile phase could result in enhanced desorption and cleanup of the packing from species in a shorter period of time. Figure 2 (top: right) analyze the effects of boundary conditions for $\kappa=0.53$. For the sake of generality Pe_z is taken as parameter. For the relatively large axial dispersion coefficients (or small Pe_z), there is a clear difference between the profiles obtained using the Dirichlet or Danckwerts boundary conditions. The more realistic Danckwerts conditions quantify the unavoidable back mixing at the column inlet and predict broader profiles. Due to the rapid radial transport, the profiles are almost identical along the radial coordinate. The sample elutes over the complete cross section with no visible radial concentration dependence, see Figure 2 (bottom: left and right).

Figures 3 and 4 provide a comparison of the analytical and numerical solutions considering injections through the inner and outer zones for less axial back mixing ($D_z=0.01cm^2/\min$ or $Pe_z=600$) and slower radial transport $\left(D_r=0.001cm^2/\min \text{ or } Pe_r=15\right)$. Both analytical and numerical solutions are compared for different values of κ. Now, significant radial transport limitations lead to still visible influence of the injection conditions at the column outlet $(x=1)$. Also the local $(\rho=0)$ and averaged concentration profiles (Eq. (37)) differ significantly at the outlet. However, for the considered high Pe_z number both Dirichlet and Danckwerts BCs produced the same results. Once again, the concentration profiles decay rapidly for large values of κ.

The plots of Figure 5 either consider the sample injection through inner core or outer ring using $\tilde{\rho}=0.707$. The radial concentration profiles are plotted at the middle of the column $(x=0.5)$ for $\tau=1.5$ using different values of the $Pe_{ratio}=\frac{R^2}{L^2}\frac{D_z}{D_r}$ and $\kappa=0.53$. Hereby, D_z was fixed at $0.3\,cm^2/\min$ and D_r was varied in the interval $D_r=[10^{-3},10^{-2},10^{-1}]cm^2/\min$. Inner (left plots) and outer (right plots) injections are compared. It can be seen that the imposed step profiles deteriorate faster for larger values of the radial transport coefficients. The two limiting cases corresponding to conservation or elimination of the injection profiles are clearly visible.

Moments of the solution profiles

In this study, plots of moments using the Danckwerts BCs are presented. The Dirichlet BCs produced similar results and are therefore omitted.

Figure 6 displays the normalized local moments $\mu_i(\rho)/\mu_0(\rho)$ (c.f. Eq. (41)) plotted along the radial coordinate of the column for $\kappa=0.53$. The effect of radial dispersion coefficient on the first, second, third and fourth moments can be clearly seen. Here, $D_z=0.3cm^2/\min$ and $u=1.5\,cm/\min$ were kept fixed and varied was the ratio $Pe_{ratio}=R^2D_z/L^2D_r$, which corresponds to $D_r=[10^{-3},10^{-2},10^{-1}]$. The plots of this figure show that moments approach to constant values along the radial coordinate for smallest value of Pe_{ratio} or largest D_r. For the smallest value of $Pe_{ratio}=0.075$, the results obtained correspond to the 1D case. Since the concentration is injected via the inner cylindrical core, all moments do not change close to the column center. The changes clearly occur in the outer section. Although, trends of the moments are similar, on inspecting closer the y-axis, the magnitudes reveal that higher moment change more significantly with changing the Pe_{ratio}. Similar trends were also observed in the case of injection through outer zone.

Figure 7 displays the local moments $\mu_i(\rho)$ (c.f. Eq. (41)) plotted along the radial coordinate of the column for three different values of dimensionless reaction constant κ. The effect of radial dispersion coefficient on the first, second, third and fourth moments can be clearly seen. Here, $D_z=0.01cm^2/\min$, $u=1.5cm/\min$ and $D_r=0.001cm^2/\min$. The plots of this figure show that values of the moments reduces on increasing κ. Since the concentration is injected via the inner cylindrical core, all moments have high values in the inner zone. Although, trends of the moments are similar, on inspecting closer the y-axis, the magnitudes reveal that higher moments have large values. Moreover, all moments have similar behaviors for all three values of κ but have different magnitudes. Similar trends were also observed in the case of injection through outer zone.

Figure 8 gives the plots of averaged first, second, third and fourth central moments as functions of flow rate. These averaged moments are obtained using the relations in Eqs. (44) and Eq. (45). The concentration was injected though inner zone. The first moment has larger value for higher velocity and has smaller value for lower speed. On the other hand, central moments shows increasing behavior in certain range of interstitial velocity and decreasing behavior in the other range of interstitial velocity.

Comparison of theoretical and experimental results

To test the applicability of our derived analytical solutions, we use the experimental data of [43]. Only a brief description of the experiment is given here, full details can be found in [43]. A conservative tracer, tritium, was injected into a saturated column over a finite period of time and relative (c/c_{inj}) profile was obtained at $z=8\,m$ downstream. In our analytical solutions, we have used $L=8\,m,\quad u=1.15\,m/hr,\quad a=2.3,\quad t_{inj}=0.217\,hr,$

$D_z = 0.031\, m/hr^2$, $D_r = 0.03\, m/hr^2$, $\varepsilon = 0.25$, $\mu = 0\ hr^{-1}$, $c_{inj} = 7\ g/l$, and inner zone injection. The Dirichlet BCs are used in this case study. A comparison of analytical and experimental results at the center of the column is shown in Figure 9. The nearly symmetrical profiles suggest that packing material inside the column was uniform. Our analytical solution is in good agreement with the experimental results. Moreover, our analytical solution is also in good agreement with the theoretical predications presented in [43,44].

6. Conclusions

We have derived general analytical solutions of a two-dimensional model describing the transport of a solute in a fixed-bed reactor of cylindrical geometry. General analytical solutions were derived through successive implementation of the finite Hankel and Laplace transforms assuming constant flow rates, linear adsorption isotherms, two sets of boundary conditions, first order decay or desorption-like reaction, and injections through inner and outer regions of the column inlet cross section. The developed analytical solutions illustrate the influence of longitudinal and radial dispersions and linear reaction. For further analysis of the solute transport behavior, the temporal moments up to the fourth order were derived from the Laplace-transformed solutions. The analytical solutions were compared for validation with the numerical solutions using a high resolution flux-limiting finite volume scheme. Typical examples of calculated concentration distributions and moments for the considered two sets of boundary conditions were presented and briefly discussed. The suggested mathematical model and derived analytical solutions could be used to describe, at a laboratory scale, desorption process in chromatography, experimental practices adopted for soil characterization, as well as transport parameters estimation and kinetic studies. Since the model takes into account dispersion, advection and a first-order chemical reaction, it is possible to use this model to estimate both the longitudinal and transverse dispersion coefficient and other parameters by fitting the data coming from experiments. Furthermore, the available analytical solutions could be used to perform sensitivity analysis and to validate numerical algorithms.

References

[1] Villermaux, J., Rodrigues, A.E., Tondeur, D. (Eds.), 1981. The chromatographic reactor in percolation processes: theory and application. Sijthoffen Noordhoff, Alpena an den Rijn, The Netherlands, 539.

[2] Ganetsos, G., Barker, P.E., 1993. Preparative and production scale chromatography. Vol. 61, Marcel Dekker, Inc., New York.

[3] Sardin, M., Schweich, D, Villermaux, J., Ganetsos, G., Barker, P.E. (Eds.), 1993. Preparative fixed-bed chromatographic reactor, preparative and production scale chromatography. Marcel Dekker Inc., New York, USA, 477.

[4] Borren, T., Fricke, J., 2005. Schmidt-Traub, H. (Eds.). Chromatographic reactors in preparative chromatography of fine chemicals and pharmaceutical agents. Wiley-VCH Verlag: Weinheim, 2005, 371.

[5] Fricke, J., Schmidt-Traub, H., Kawase, M., 2005. Chromatographic reactor, Ullmann's encyclopedia of industrial chemistry. Wiley-VCH Verlag: Weinheim, 2005.

[6] Carta, G., 1988. Exact analytical solution of a mathematical model for chromatographic operations. Chem. Eng. Sci. 43, 2877-2883.

[7] D. M. Ruthven, Principles of adsorption and adsorption processes, Wiley-Inter science, New York, 1984.

[8] G. Guiochon, A. Felinger, D. G. Shirazi, A. M. Katti, Fundamentals of preparative and nonlinear chromatography, 2nd ed., Elsevier, San Diego, USA, 2006.

[9] van Genuchten, M.Th., Alves, W.J., 1982. Analytical solutions of the one-dimensional convective dispersive solute transport equation. US Department of Agriculture, Technical Bulletin No. 1661, 151-300.

[10] Batu, V., 1989. A generalized two-dimensional analytical solution for hydrodynamic dispersion in bounded media with the first-type boundary condition at the source. Water Resour. Res. 25, 1125-1132.

[11] Batu V., 1993. A generalized two-dimensional analytical solute transport model in bounded media for flux-type finite multiple sources. Water Resour. Res. 29, 288192.

[12] Coimbra, M.C., Sereno, C., Rodrigues, A., 2003.A moving finite element method for the solution of two-dimensional time-dependent models. Appl. Num. Math. 44, 449-469.

[13] Leij, F.J., Skaggs, T.H., van Genuchten M.Th., 1991.Analytical solution for solute transport in three-dimensional semi-infinite porous media. Water Resour. Res. 27, 271933.

[14] Park, E., Zhan, H., 2001. Analytical solutions of contaminant transport from finite one-, two, three-dimensional sources in a finite-thickness aquifer. J. Contam. Hydrol.53, 4161.

[15] Zhang, X., Qi, X., Zhou, X., Pang, H., 2006. An in situ method to measure the longitudinal and transverse dispersion coefficients of solute transport in soil. J. Hydrol. 328, 6149.

[16] Massab´o, M., Cianci, R., Paladino, O., 2006. Some analytical solutions for two dimensional convection dispersion equation in cylindrical geometry. Environ. Modell. Softw. 21, 6818.

[17] Massab`o, M., Catania, F., Paladino, O., 2011. Exact analytical solutions for two dimensional advection dispersion equation in cylindrical coordinates subject to third type inlet boundary condition. Adv. Water Resour. 34, 365374.

[18] Chen, J.-S., Liu, Y.-H., Liang, C.-P., Liu, C.-W., Lin, C.-W., 2011. Exact analytical solutions for two-dimensional advection dispersion equation in cylindrical coordinates

subject to third-type inlet boundary conditions. Adv. Water Resour. 34, 365-374.
[19] Chen, J.-S., Liu, Y.-H., Liang, C.-P., Liu, C.-W., Lin, C.-W., 2011. Analytical solutions to two-dimensional advection dispersion equation in cylindrical coordinates in finite domain subject to first- and third-type inlet boundary conditions. J. Hydrol. 405, 522-531.
[20] Qamar, S., Khan, F.U., Mehmood, Y., Seidel-Morgenstern, A., 2014. Analytical solution of a two-dimensional model of liquid chromatography including moment analysis, Chem. Eng. Sci. 116, 576-589.
[21] Grane, F.E., Gardner, G.H.F., 1961. Measurements of transverse dispersion in granular media, J. Chem. Eng. Data 6, 283-287.
[22] Simpson, E.S., 1962. Transverse dispersion in liquid flow through porous media. Prof. pap. 411-c, U.S. Geological Survey, Washington, DC.
[23] Robbins, G.A., 1989. Methods for determining transverse dispersion coefficients ofporous media in laboratory column experiments. Water Resour, Res. 25, 1249-1258.
[24] Pisani, S., Tosi, N., 1994. Two methods for the laboratory identification of transversal dispersivity, Ground Water 32, 431-438.
[25] Aris, R., 1958. On the dispersion of linear kinematic waves, Proc. R. Soc. Londan, Ser. A 245:268-277.
[26] Antos, D., Kaczmarski, K., Wojciecha, P., Seidel-Morgenstern, A., 2003. Concentration dependence of lumped mass transfer coefficients: Linear versus non-linear chromatography and isocratic versus gradient operation. J. Chromatogr. A 1006, 61-76.
[27] Kubin, M., 1965. Beitrag zur Theorie der Chromatographie. Collect. Czech. Chem. Commun. 30, 1104-1118.
[28] Kubin, M., 1965. Beitrag zur Theorie der Chromatographie. 11. Einfluss der Diffusion Ausserhalb und der Adsorption Innerhalb des Sorbens-Korns. Collect. Czech. Chem. Commun. 30, 2900-2907.
[29] Kucera, E., 1965. Contribution to the theory of chromatography: Linear non-equilibrium elution chromatography. J. Chromatogr. A 19, 237-248.
[30] Lenhoff, A.M., 1987. Significance and estimation of chromatographic parameters. J. Chromatogr. A 384, 285-299.
[31] Miyabe, K., Guiochon, G., 2000. Influence of the modification conditions of alkyl bonded ligands on the characteristics of reversed-phase liquid chromatography. J. Chromatogr. A 903, 1-12.
[32] Miyabe, K., Guiochon, G., 2003. Measurement of the parameters of the mass transfer kinetics in high performance liquid chromatography. J. Sep. Sci. 26, 155-173.
[33] Miyabe, K., 2007. Surface diffusion in reversed-phase liquid chromatography using silica gel stationary phases of different C1 and C18 ligand densities. J. Chromatogr. A 1167, 161-170.
[34] Miyabe, K., 2009. Moment analysis of chromatographic behavior in reversed-phase liquid chromatography. J. Sep. Sci. 32, 757-770.
[35] Schneider, P., Smith, J.M., 1968. Adsorption rate constants from chromatography. A.I.Ch.E. J. 14, 762-771.
[36] Suzuki, M., 1973. Notes on determining the moments of the impulse response of the basic transformed equations. J. Chem. Eng. Japan 6, 540-543.
[37] Wolff, H.-J., Radeke, K.-H, Gelbin, D., 1980. Heat and mass transfer in packed beds- IV use of weighted moments to determine axial dispersion coefficient. Chem. Eng. Sci. 34, 101-107.
[38] Wolff, H.-J., Radeke, K.-H, Gelbin, D., 1980. Weighted moments and the pore diffusion model. Chem. Eng. Sci. 35, 1481-1485.
[39] Javeed, S., Qamar, S., Ashraf, W., Seidel-Morgenstern, A., Warnecke, G., 2013. Analysis and numerical investigation of two dynamic models for liquid chromatography. Chemical Engineering Science 90, 17-31.
[40] Parveen, S., Qamar, S., Seidel-Morgenstern, A., 2015. Two-dimensional non-equilibrium model of liquid chromatography: analytical solutions and moment analysis. Chem. Eng. Sci. 122, 64-77.
[41] Javeed, S., Qamar, S., Seidel-Morgenstern, A., Warnecke, G., 2011. Efficient and accurate numerical simulation of nonlinear chromatographic processes. Comput. & Chem. Eng. 35, 2294-2305.
[42] Rice, R.G.; Do, D.D. Applied mathematics and modeling for chemical engineers. Wiley-Interscience, New York, 1995.
[43] Pang, L; Hunt, B., 2001. Solutions and verification of a scale dependent dispersion model. J. Contam. Hydrol. 53, 21-39.
[44] Su, N.; Sander, G.C.., Lie, F; Anh, V.; Barry, D.A., 2005. Similarity solutions for solute transport in fractional porous media using a time- and scale-dependent dispersivity. Appl. Math. Model. 29, 852-870.

Table 1: Parameters used in the considered test problems.

Parameters	values
Column length	$L = 4\ cm$
Column radius	$R = 0.2\ cm$
Radius of inner zone	$\tilde{r} = 0.1414\ cm$
Porosity	$\epsilon = 0.4$
Interstitial velocity	$u = 1.5\ cm/min$
Axial dispersion coefficient	$D_z = [0.01, 0.3]\ cm^2/min,\ \ Pe_z = [20, 600]$
Radial dispersion coefficient	$D_r = [0.001, 0.03]\ cm^2/min,\ \ Pe_r = [0.5, 15]$
Injection time	$t_{\text{inj}} = 1\ min$
Initial concentration	$c_{\text{init}} = 0\, g/l$
Concentration at inlet	$c_{\text{inj}} = 1\, g/l$
Adsorption equilibrium constant	$a = 1$

Note That: $Pe_{ratio} = \dfrac{R^2 D_z}{L^2 D_r} = Pe_r / Pe_z$.

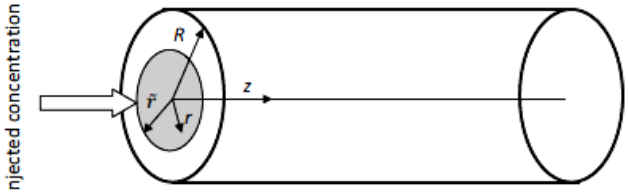

Figure 1: Schematic representation of a chromatographic column of cylindrical geometry

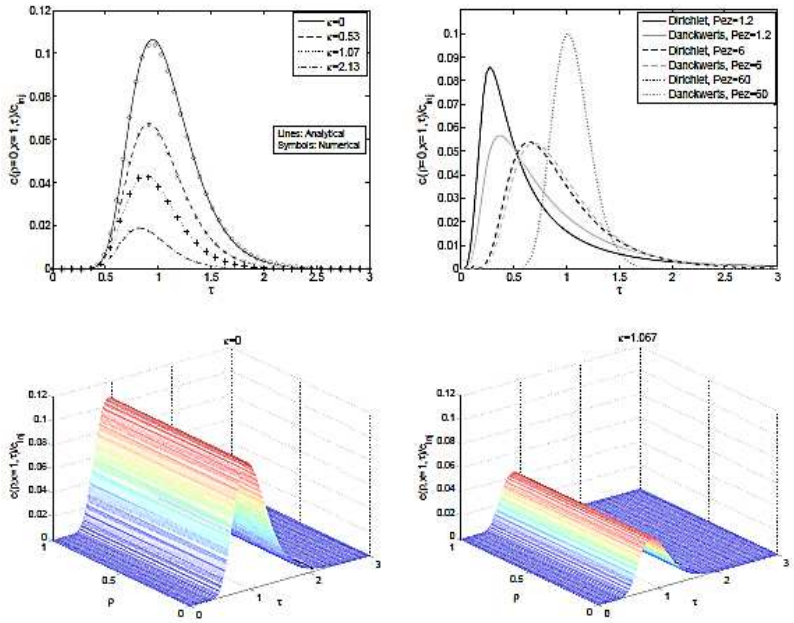

Figure 2: Injection through inner zone. Comparison of solutions for different values of κ and Pe_z with fixed $Pe_r = 0.5$. Other parameters are given in Table 1.

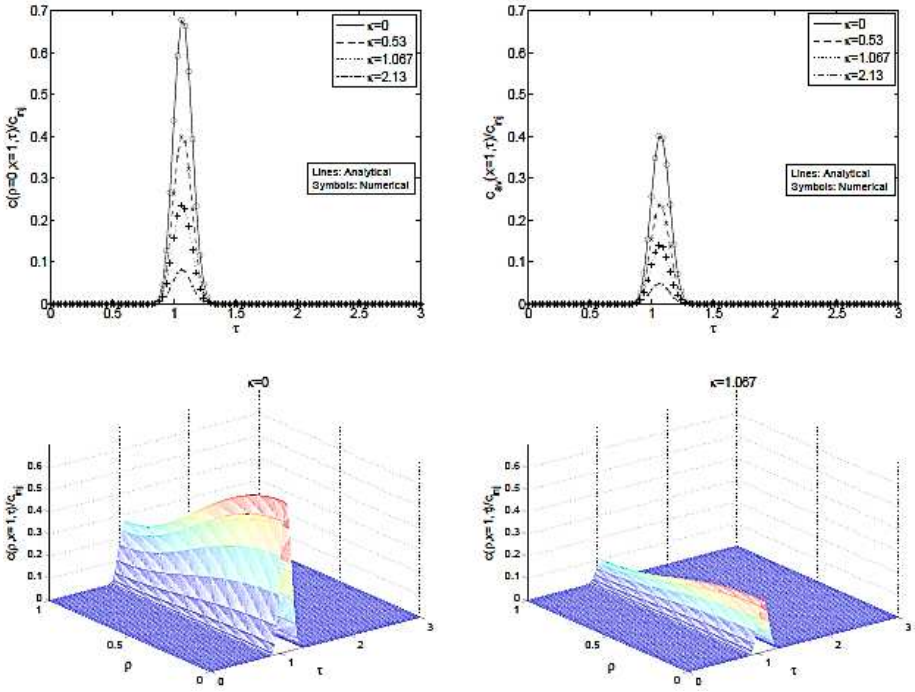

Figure 3: Injection through inner zone. Comparison of solutions for different values of κ with fixed $Pe_z = 600$ and $Pe_r = 15$. Other parameters are given in Table 1.

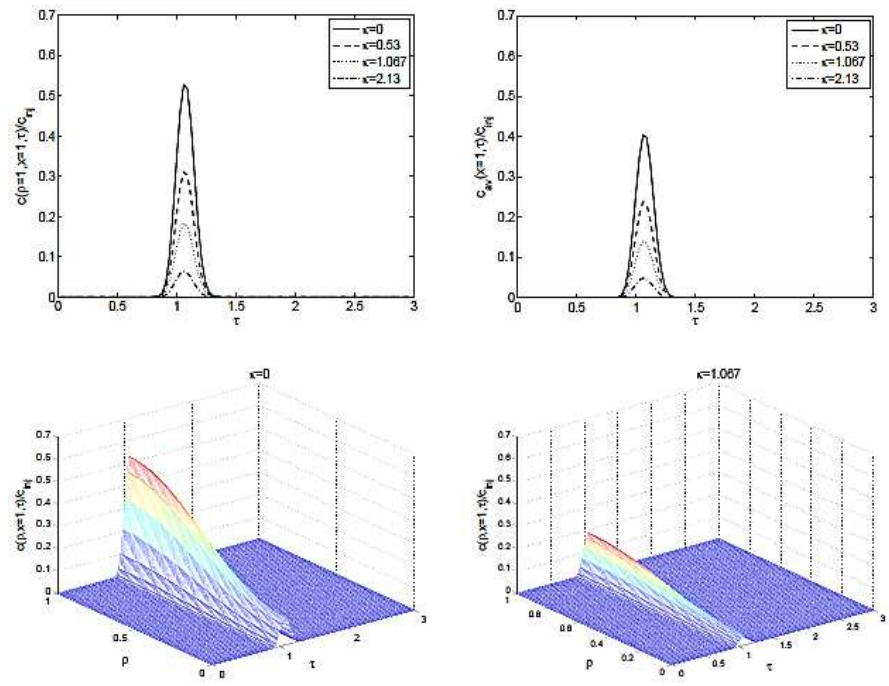

Figure 4: Injection through outer annular zone. Comparison of solutions for different values of κ with fixed $Pe_z = 600$ and $Pe_r = 15$. Other parameters are given in Table 1.

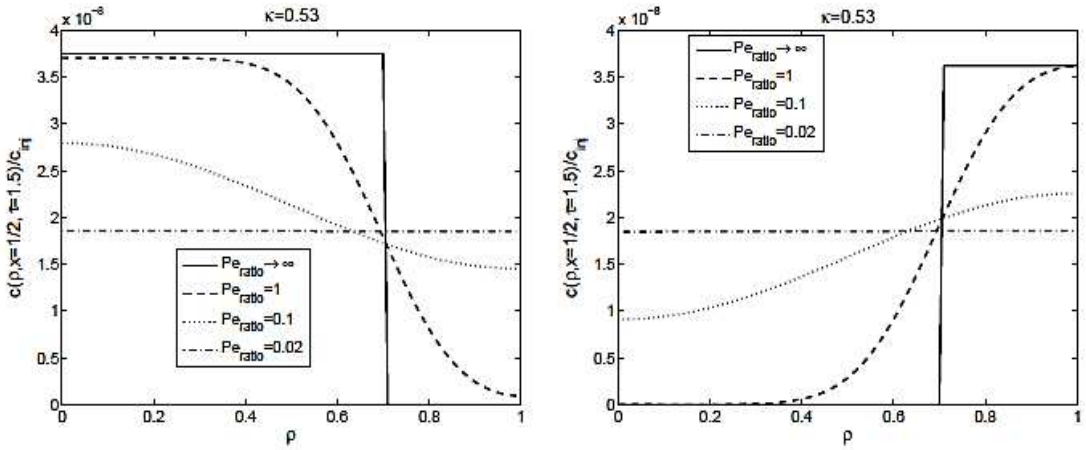

Figure 5: Comparison of solutions for different values of $Pe_{ratio} = R^2 D_z / L^2 D_r$ with fixed $Pe_z = 600$ and $\kappa = 0.53$. Left: inner zone injection, right: outer zone injection. Other parameters are given in Table 1.

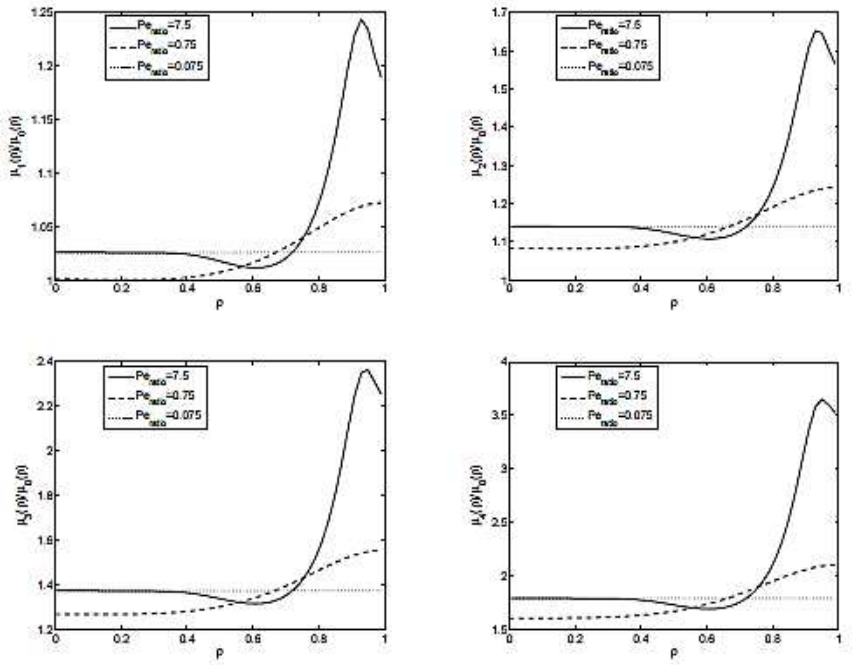

Figure 6: Inner zone injection: Effect of D_r on the local moments $\mu_i(\rho)$ (c.f. Eq.(41)) for fixed $D_z = 0.3cm^2/\min$ ($Pe_z = 20$) and $\kappa = 0.53$. Varied is the ratio $Pe_{ratio} = R^2 D_z / L^2 D_r$. Table 1 gives other parameters.

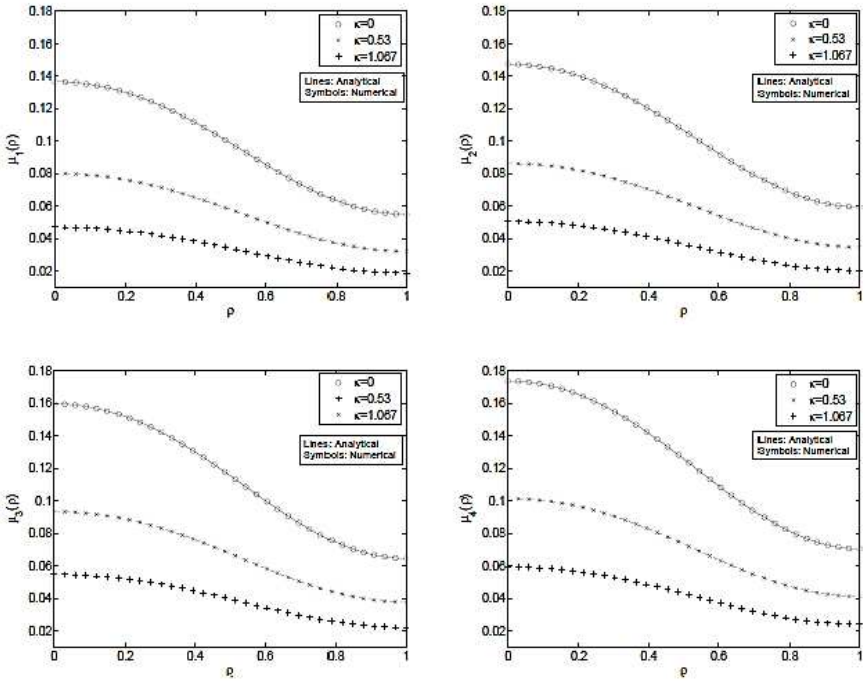

Figure 7: Inner zone injection: Comparison of analytical and numerical moments for different values of κ and fixed $D_z = 0.01cm^2/\min$ and $D_r = 0.001cm^2/\min$. Other parameters are given in Table 1.

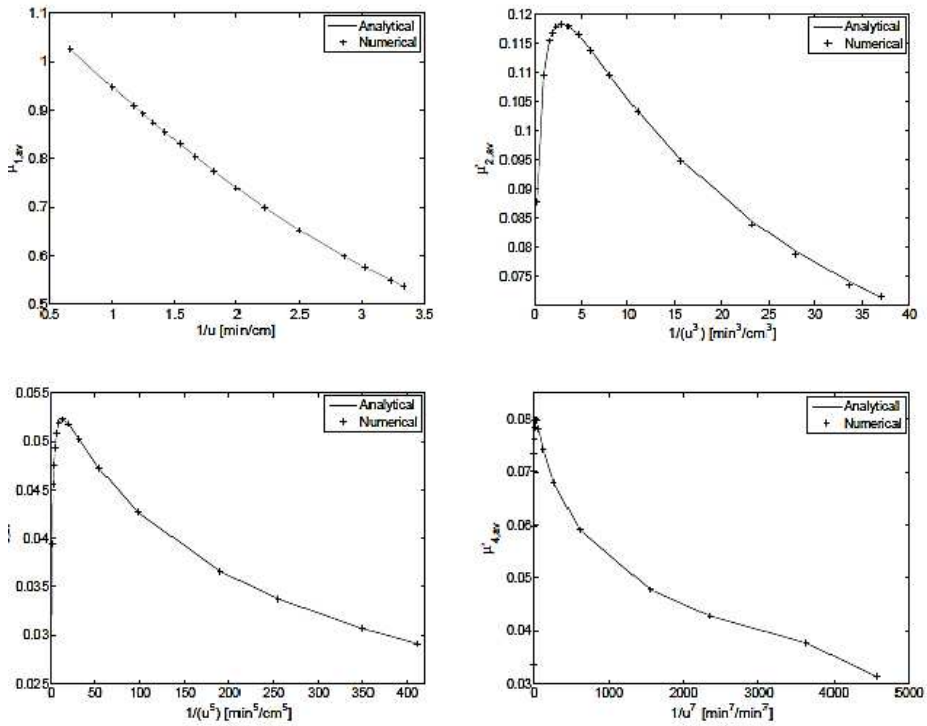

Figure 8: Inner zone injection: Comparison of analytical and numerical averaged central moments for $D_z = 0.3\,cm^2/\min$ and $D_r = 0.03\,cm^2/\min$ and $\mu = 0.2\,\min^{-1}$. Other parameters are given in Table 1.

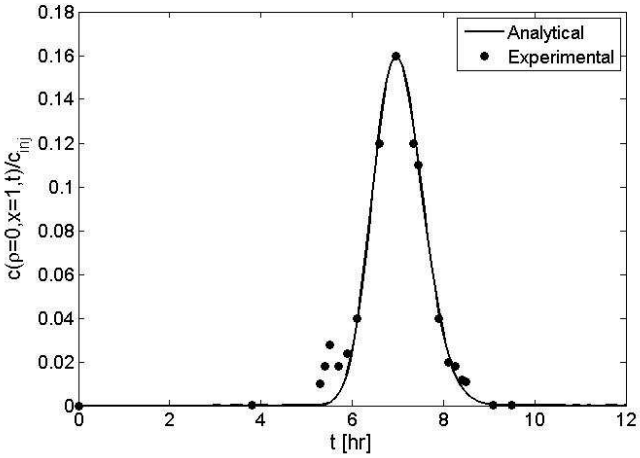

Figure 9: A comparison of analytical and numerical experimental results.